Linear stability analysis for the differentially heated rotating annulus

Gregory M. Lewis and Wayne Nagata [1]

Keywords: differentially heated rotating fluid experiment, axisymmetric to non-axisymmetric transition, numerical computation of eigenvalues

Abstract

We use linear stability analysis to approximate the axisymmetric to non-axisymmetric transition in the differentially heated rotating annulus. We study an accurate mathematical model that uses the Navier-Stokes equations in the Boussinesq approximation. The steady axisymmetric solution satisfies a two-dimensional partial differential boundary value problem. It is not possible to compute the solution analytically, and so numerical methods are used. The eigenvalues are also given by a two-dimensional partial differential problem, and are approximated using the matrix eigenvalue problem that results from discretizing the linear part of the appropriate equations.

A comparison is made with the experimental results of Fein (1973). It is shown that the predictions using linear stability analysis accurately reproduce many of the experimental observations. Of particular interest is that the analysis predicts cusping of the axisymmetric to non-axisymmetric transition curve at wave number transitions, and the wave number maximum along the lower transition curve is accurately determined. The correspondence between theoretical and experimental results validates the numerical approximations as well as the application of linear stability analysis.

1 Introduction

Eigenvalues have long been used as a tool for theoretically predicting the stability of fluid flows. They can be used to quantitatively delineate the regions in parameter space where a steady flow is linearly stable from regions where it is unstable. In fact, under suitable conditions, it can be shown that if a flow is linearly stable then it is indeed a stable flow, even when nonlinearity is considered. In addition, linear stability analysis is the first step in

[1] both of the Department of Mathematics, University of British Columbia, Vancouver, BC, V6T 1Z2, Canada

a nonlinear bifurcation analysis that can be used to discover new solutions of the dynamical equations.

In most previous work, linear stability analysis is used to study the stability of a basic steady flow for which the corresponding steady solution of the model equations can be written as an analytical expression. However, analytical methods are sometimes not sufficient to determine the eigenvalues, and, in such cases, numerical approximations are necessary. These studies have concentrated on cases where the linear stability analysis can be reduced to an ordinary differential (one-dimensional) eigenvalue problem. Thus, even when numerical methods must be implemented, it is not computationally intensive to find accurate approximations for the eigenvalues. However, there are many interesting flows for which the corresponding steady solution cannot be found analytically and for which the corresponding eigenvalue problem cannot be reduced to a one-dimensional problem. Linear stability analysis of such flows is often not considered, because it is not known if, due to computer limitations, sufficiently fine numerical resolution can be attained to produce valid results.

Even when it can be performed, linear stability analysis may still not accurately reproduce experimental results. For example, in Poiseuille flow, experimental observations indicate that instability sets in for significantly lower parameter values than the linear stability analysis predicts (Maslowe, 1985; Trefethen et al., 1993). The cause of this has been attributed to the non-orthogonality of the eigenfunctions, due to the linearization of the dynamical equations about the steady solution being a non-normal operator[2] (Trefethen et al., 1993; Farrell and Ioannou, 1996). Such operators often result, for instance, when considering steady flows with nonlinear spatial variations. In problems involving non-normal operators, it is possible that even when the steady solution is linearly stable, small perturbations (that are present in all physical systems) can grow to appreciable size before they ultimately decay. Thus, small perturbations may take the flow into some regime where the linearization is not valid.

The success of linear stability analysis, for example, in the application to Rayleigh-Bénard convection (see *e.g.* Chandrasekhar, 1961) has been attributed to the normality of the linearization of the dynamical equations about the relevant steady flow. However, linear stability analysis does not always fail in cases involving non-normal operators. For example, in the Couette-Taylor problem (Chossat and Iooss, 1994), linear stability analysis successfully predicts experimentally observed transitions between different flow regimes. In fact, the most prominent failure of linear stability analysis seems to be in its application to parallel shear flows, and it is possible that non-normality is only an issue when considering operators that are, in some sense, "far from normal" (Trefethen, 1997).

Here, we use linear stability analysis to approximate the transition from axisymmetric to

[2]A normal operator is defined as an operator A that satisfies $AA^* = A^*A$, where A^* is the adjoint of A; an operator is normal if and only if all its eigenfunctions are mutually orthogonal.

non-axisymmetric flow in the differentially heated rotating annulus. The steady solution of the model equations that corresponds to the axisymmetric flow cannot be found analytically, and must be approximated from a discretization of a two-dimensional partial differential boundary value problem. In addition, the eigenvalue problem can only be reduced to a two-dimensional partial differential problem, that also must be solved numerically. Furthermore, although the steady axisymmetric flow is not a parallel shear flow, the linearization of the model equations about the corresponding steady solution is not a normal operator. Therefore, it is not known *a priori* if linear stability analysis will give accurate predictions. For this reason, we make a detailed quantitative comparison between the predictions we obtain using linear stability analysis and the experimental observations of Fein (1973). We study an accurate mathematical model, with the intent of minimizing errors due to the model, so that it can be argued that any substantial discrepancies between the theoretical and experimental results can be attributed to either errors in the numerical approximations or the failure of linear stability analysis.

In Section 7, we present our results, and show that, for this application, linear stability analysis is indeed successful in predicting the experimental observations. The remainder of the paper is arranged as follows. In the next section, we describe the differentially heated rotating annulus experiments and in so doing, give more detail of the problem we will be addressing. In Section 3, we discuss linear stability analysis in a general context. We write down the model equations in Section 4, while in Section 5, the eigenvalue problem for the present application is derived. The numerical methods are discussed in Section 6. A conclusion follows the results section.

2 Experimental observations

Many laboratory experiments have studied the fluid flow in a rotating cylindrical annulus, where a differential heating is obtained by keeping the inner and outer walls of the annulus at different temperatures. See Figure 1. The experiments consist of finding the various stable flow patterns that occur at different values of the rotation rate and differential heating. Usually, the results are presented in a diagram where the transitions between the different flow types are plotted on a graph with coordinate axes being the Taylor number $\mathcal{T}$ and the thermal Rossby number $\mathcal{R}$, which are judged to be the two most important dimensionless parameters (Fein, 1973; Hide and Mason, 1975). The Taylor number

$$\mathcal{T} = \frac{4\Omega^2 R^4}{\nu^2} \tag{1}$$

is a measure of the relative importance of rotation to viscosity, where Ω is the rate of rotation, $R = r_b - r_a$ is the difference between the outer and inner radii of the annulus, and ν is the

kinematic viscosity of the fluid. The thermal Rossby number

$$\mathcal{R} = \frac{\alpha g D \Delta T}{\Omega^2 R^2} \tag{2}$$

is a measure of the relative importance of rotation to the differential heating, where $\Delta T = T_b - T_a$ is the imposed horizontal temperature gradient, α is the coefficient of thermal expansion, D is the depth of the fluid, and g is the gravitational acceleration. Here, we consider $\Delta T > 0$; the inner wall of the annulus is held at a lower temperature than the outer wall. If all other parameters are held fixed, there is a one-to-one relationship between the dimensionless parameters (thermal Rossby number and the Taylor number) and the physical parameters (the differential heating and rate of rotation).

The experiments generally find four main flow regimes in different regions of parameter space (see Figure 2): (1) **Axisymmetric flow**, characterized by its azimuthal invariance. (2) **Steady waves**, a non-axisymmetric flow that resembles rotating waves with constant amplitude and phase. Different wavelengths are seen in different subregions, with the possibility of observing stable waves of different wavelengths within the same subregion. The transitions between the subregions exhibit hysteresis. (3) **Vacillation**, where the amplitude or wavelength of the observed wave varies apparently periodically in time. (4) **Irregular Flow**, characterized by its irregular nature in both space and time. All of the observed flows have their counterparts in the atmosphere (Hide and Mason, 1975; Ghil and Childress, 1987).

Of particular interest to us, is the transition from the axisymmetric to wave regime. For small values of the differential heating and rotation rate, a steady axisymmetric pattern is observed. As the parameters are increased, this relatively simple pattern becomes unstable and a wave motion is observed. Below, we reproduce the transition curve between axisymmetric and wave regimes by studying the linear stability of the axisymmetric flow.

3 Linear stability analysis

The linear stability of a steady solution is defined in terms of the eigenvalues of the linearization of the dynamical equations about that solution. If the real parts of *all* the eigenvalues are negative, then all small perturbations from the steady solution will decay in the linearized equations. In this case, the solution is said to be linearly stable. If any of the eigenvalues has positive real part, then some small perturbations will grow, and the solution is linearly unstable. If there are only eigenvalues with zero real part and negative real part, it is called neutrally stable, because there is neither growth nor decay of some small perturbations. The curves in the space of parameters that indicate the parameter values where the solution is neutrally stable are called neutral stability curves. These are very useful because, generally,

they are the boundaries between the regions in parameter space where the steady solution of interest is linearly stable and those regions where it is linearly unstable.

Linear stability analysis is justified by the Hartman-Grobman theorem (for a precise statement of the theorem in the context of partial differential equations, see *e.g.* Henry, 1981, or in the context of ordinary differential equations, see *e.g.* Wiggins, 1990). A hyperbolic steady solution is one whose linearization has no eigenvalues with zero real part. The Hartman-Grobman theorem states that if the steady solution is hyperbolic, then the linearization about the solution has qualitatively the same behaviour as the full nonlinear system. This implies that if the steady solution is linearly stable, then it is indeed a stable solution. More precisely, if a steady solution is *linearly* stable, then there is a neighbourhood about that solution where all initial conditions for the *nonlinear* system will produce solutions that tend to the steady solution as $t \to \infty$. However, this definition of stability gives only the long-time behaviour ($t \to \infty$) and says nothing about transient behaviour. Also, the theorem does not state the size of the neighbourhood about the steady solution, and so it could be that the size of the neighbourhood is very small. If this is the case, then the natural fluctuations present in physical systems may be large enough to take the system out of the neighbourhood, and a linearly stable solution may not correspond to a physically observable flow. The size of the neighbourhood depends on the specific equations and solution, and it is possible that the non-normality of the linearization of the equations about the given solution causes a significant decrease in the size of the neighbourhood.

A different method of analysis that is often used to numerically determine the stability of a solution could be called 'numerical experimentation', since the procedure of the laboratory experiments is simulated on a numerical model. The procedure often begins by finding a steady solution either analytically or numerically. This solution, to which small amplitude random perturbations are added to simulate natural fluctuations, is used as the initial condition for a numerical integration, or time-stepping. If the time-stepping produces solutions that seem to stay near the steady solution, then the steady solution is labelled as stable in these studies. The parameters are then varied and the process is repeated. If the time-stepping produces a solution that evolves away from the steady solution, it is labelled unstable. In this case, the time-stepping is continued until transient behaviour disappears and the system appears to reach a different stable steady state, periodic solution, or a more complicated solution.

Many different models have been studied using numerical experimentation. Mo et al. (1995) followed the above procedure on a three-dimensional quasigeostrophic model with Ekman layers at the top and bottom. James et al. (1981), Hignett et al. (1985), Miller and Butler (1991) and Lu et al. (1994) performed numerical experiments with a Navier-

Stokes model in cylindrical geometry for direct comparison to laboratory experiments. The geometry of the annulus that we use in the present study is the same as that of Miller and Butler (1991). Kwak and Hyun (1992) performed the analysis on a model of the Hathaway and Fowlis (1986) experiment, and Collins and James (1995) studied a simplified global circulation model. Lewis (1992) and Mundt et al. (1995) also performed time-integration of basic states on different two-layer models. This list is far from exhaustive.

However, in addition to being qualitative, numerical experimentation does not highlight the physical processes that lead to the observed dynamics. Thus, although it is a good method of validating numerical models, it is not an ideal tool for gaining insight into the physical nature of the system. Also, if the random perturbation that is added to the steady solution is too large, the initial condition may be outside the neighbourhood of attraction of the steady solution (see above) and the solution may appear to be unstable, even though the solution may be physically observable. Because long time integration is needed to determine the stability, errors are introduced at every time step.

In contrast, eigenvalues may be used to produce a quantitative, completely objective, delineation of the region of stability of a steady solution. Also, numerical approximations of the eigenvalues can be more easily verified. Finally, the information that is gained may be used in a bifurcation analysis that could lead to further understanding of the mechanisms present in the physical system. For instance, the results presented here on the differentially heated rotating annulus are the first step in a double Hopf bifurcation (two-mode weakly nonlinear) analysis (Lewis and Nagata, 2001). This analysis shows that there are regions in the parameter space where there are two stable wave solutions and it also indicates the mechanism by which the hysteresis of these solutions occurs. However, caution must still be taken, because, as discussed above, the eigenvalues do not give transient behaviour and the analysis may not accurately predict the stability of observed flows.

4 Model equations

The model consists of the Navier-Stokes equations describing the fluid motion, in a rotating reference frame, and simplified using the Boussinesq approximation. In particular, we consider the variations of all fluid properties, except the density, to be negligible and the equation of state of the fluid is assumed to be

$$\rho = \rho_0 \left(1 - \alpha \left(T - T_0\right)\right) \tag{3}$$

where ρ is the density of the fluid, T is the temperature, α is the (constant) coefficient of thermal expansion, and ρ_0 is the density at a reference temperature T_0. The dimensionless quantity $\alpha \left(T - T_0\right)$ is assumed to be small. A significant simplification due to the Boussinesq

approximation is that the fluid can be considered to be incompressible. The boundaries are the inner and outer walls of the cylindrical annulus, as well as a rigid flat top and bottom. At the boundaries, the no-slip condition is imposed on the fluid, and the temperature is T_a and T_b at the inner and outer walls, respectively. The bottom and top are thermally insulating. The equations are written in circular cylindrical coordinates in a frame of reference co-rotating at rate Ω with the annulus. The radial, azimuthal and vertical (or axial) coordinates are denoted r, φ and z, respectively, with unit vectors $\mathbf{e}_r$, $\mathbf{e}_\varphi$ and $\mathbf{e}_z$. See Figure 1.

The equations describing the evolution of the vector fluid velocity, $\mathbf{u} = \mathbf{u}(r, \varphi, z, t) = u\mathbf{e}_r + v\mathbf{e}_\varphi + w\mathbf{e}_z$ and the temperature of the fluid, $T = T(r, \varphi, z, t)$ are:

$$\frac{\partial \mathbf{u}}{\partial t} = \nu\nabla^2\mathbf{u} - 2\Omega\mathbf{e}_z \times \mathbf{u} + \left(g\mathbf{e}_z - \Omega^2 r\mathbf{e}_r\right)\alpha\,(T - T_0) - \frac{1}{\rho_0}\nabla p - (\mathbf{u}\cdot\nabla)\,\mathbf{u}, \tag{4}$$

$$\frac{\partial T}{\partial t} = \kappa\nabla^2 T - (\mathbf{u}\cdot\nabla)\,T, \tag{5}$$

$$\nabla\cdot\mathbf{u} = 0, \tag{6}$$

where p is the pressure deviation from $p_0 = \rho_0 g(D - z) + \rho_0\Omega^2 r^2/2$, ν is the kinematic viscosity, κ is the coefficient of thermal diffusivity, g is the gravitational acceleration, ∇ is the usual gradient operator in cylindrical coordinates, and the spatial domain is defined by $r_a < r < r_b$, $0 \le \varphi < 2\pi$, and $0 < z < D$. The values of ν and κ are chosen to be those of the fluid at the reference temperature T_0, and it is assumed that the difference between the temperature of the fluid and T_0 is everywhere small enough so that ν and κ can be considered as constants. Centrifugal buoyancy has been included since we found it to have non-negligible effects.

The boundary conditions are

$$\begin{aligned}
\mathbf{u} = 0 \quad &\text{on} \quad r = r_a, r_b \ \text{ and } \ z = 0, D,\\
T = T_a \quad &\text{on} \quad r = r_a,\\
T = T_b \quad &\text{on} \quad r = r_b,\\
\frac{\partial T}{\partial z} = 0 \quad &\text{on} \quad z = 0, D,
\end{aligned} \tag{7}$$

with 2π-periodicity in the azimuthal variable φ.

If we scale the spatial variables as

$$r \to Rr', \quad \varphi \to \varphi, \quad z \to Dz', \tag{8}$$

and write

$$T \to T' + \Delta T r' - \Delta T\frac{r_a}{R} + T_a, \tag{9}$$

where $R = r_b - r_a$ and $\Delta T = T_b - T_a$, then drop the primes, we obtain the following equations describing the evolution of the fluid velocity $\mathbf{u} = u(r,\varphi,z,t)\mathbf{e}_r + v(r,\varphi,z,t)\mathbf{e}_\varphi + w(r,\varphi,z,t)\mathbf{e}_z$, pressure deviation $p = p(r,\varphi,z,t)$ and temperature deviation $T = T(r,\varphi,z,t)$:

$$\frac{\partial \mathbf{u}}{\partial t} = \nu_s \nabla_s^2 \mathbf{u} - \frac{1}{R\rho_0}\nabla_s p - 2\Omega \mathbf{e}_z \times \mathbf{u} + \left(g\mathbf{e}_z - \Omega^2 R r \mathbf{e}_r\right)\alpha\left[T + \Delta T\left(r - \frac{r_a}{R}\right) + T_a - T_0\right] - \frac{1}{R}\left(\mathbf{u}\cdot\nabla_s\right)\mathbf{u}, \tag{10}$$

$$\frac{\partial T}{\partial t} = \kappa_s \nabla_s^2 T + \kappa_s \frac{\Delta T}{r} - \frac{\Delta T}{R}u - \frac{1}{R}\left(\mathbf{u}\cdot\nabla_s\right)T, \tag{11}$$

$$\nabla_s \cdot \mathbf{u} = \frac{\partial u}{\partial r} + \frac{u}{r} + \frac{\partial v}{\partial \varphi} + \frac{1}{\delta}\frac{\partial w}{\partial z} = 0, \tag{12}$$

where $\delta = D/R$, $\nu_s = \nu/R^2$, ν is the kinematic viscosity, $\kappa_s = \kappa/R^2$, κ is the coefficient of thermal diffusivity, g is the gravitational acceleration,

$$\nabla_s^2 = \frac{\partial^2}{\partial r^2} + \frac{1}{r}\frac{\partial}{\partial r} + \frac{1}{r^2}\frac{\partial^2}{\partial \varphi^2} + \frac{1}{\delta^2}\frac{\partial^2}{\partial z^2},$$

$$\nabla_s = \mathbf{e}_r\frac{\partial}{\partial r} + \mathbf{e}_\varphi\frac{1}{r}\frac{\partial}{\partial \varphi} + \mathbf{e}_z\frac{1}{\delta}\frac{\partial}{\partial z},$$

$$\left(\mathbf{u}\cdot\nabla_s\right)\mathbf{u} = \left[\left(\mathbf{u}\cdot\nabla_s\right)u - \frac{v^2}{r}\right]\mathbf{e}_r + \left[\left(\mathbf{u}\cdot\nabla_s\right)v + \frac{uv}{r}\right]\mathbf{e}_\varphi + \left[\left(\mathbf{u}\cdot\nabla_s\right)w\right]\mathbf{e}_z, \tag{13}$$

and

$$\left(\mathbf{u}\cdot\nabla_s\right)f = u\frac{\partial f}{\partial r} + \frac{v}{r}\frac{\partial f}{\partial \varphi} + \frac{1}{\delta}w\frac{\partial f}{\partial z} \tag{14}$$

for any scalar function $f = f(r,\varphi,z,t)$. The domain is now expressed as $r_a/R < r < r_b/R$, $0 \le \varphi < 2\pi$, $0 < z < 1$, and the boundary conditions are

$$\begin{aligned} \mathbf{u} &= 0 \quad \text{on} \quad r = \frac{r_a}{R},\ \frac{r_b}{R} \ \text{ and } \ z = 0, 1, \\ T &= 0 \quad \text{on} \quad r = \frac{r_a}{R},\ \frac{r_b}{R}, \\ \frac{\partial T}{\partial z} &= 0 \quad \text{on} \quad z = 0, 1, \end{aligned} \tag{15}$$

with 2π-periodicity in φ for $\mathbf{u}$, T and p.

If the equations were written completely in terms of dimensionless variables, then the Taylor number $\mathcal{T}$, the thermal Rossby number $\mathcal{R}$, and other dimensionless parameters would enter the equations. However, this would not simplify the analysis and so we choose to work with the equations in the form (10) – (12). The parameters of interest are the rotation rate Ω and the temperature difference ΔT between the inner and outer annulus walls, because these are the quantities (external variables) which are generally varied in an experiment. We present our results in terms of $\mathcal{T}$ and $\mathcal{R}$ so that they may be easily compared to the experimental results.

5 The analysis

The analysis consists of finding the locations in the $(\Omega,\ \Delta T)$ parameter space where the steady axisymmetric solution is neutrally stable. These locations form the neutral stability curves. The main steps for plotting the curves are as follows:

1. Calculate the steady axisymmetric solution at a particular location in parameter space.
2. Solve the eigenvalue problem for this solution to find its linear stability.
3. Repeat steps (1) and (2) at various locations in parameter space to find the parameter values where the solution is neutrally stable.

The eigenvalues cannot be computed analytically and are therefore approximated numerically. An analytical form for the steady axisymmetric solution is also not known and so this too has to be approximated numerically. In the analysis, this is dealt with by leaving the axisymmetric solution unresolved in the perturbation equations (see Section 5.2). Then, for the numerical approximation of the eigenvalues, the values of the axisymmetric solution are only needed at specific spatial locations (the grid points), and numerical approximations are used.

In the remainder of this section, we discuss the equations that must be derived in order to calculate the eigenvalues. We discuss the numerical approximations in Section 6.

5.1 Steady axisymmetric solution

The analysis begins with the computation of a steady axisymmetric solution. That is, we look for solutions of (10) – (12), satisfying the boundary conditions (15), in the form

$$u = u^{(0)}(r,z), \quad v = v^{(0)}(r,z), \quad w = w^{(0)}(r,z), \quad T = T^{(0)}(r,z), \tag{16}$$

where the dependent variables are independent of φ and t. Although it is not written explicitly, the solutions also depend on the parameters.

Stream functions are used to solve for the axisymmetric solutions. With the form of the solutions as above, the incompressibility equation (12) becomes

$$\frac{\partial u^{(0)}}{\partial r} + \frac{u^{(0)}}{r} + \frac{1}{\delta}\frac{\partial w^{(0)}}{\partial z} = 0. \tag{17}$$

If $u^{(0)}$ and $w^{(0)}$ are written in terms of a stream function ξ, defined by

$$u^{(0)} = \frac{1}{r}\frac{\partial \xi}{\partial z}, \qquad w^{(0)} = -\delta\frac{1}{r}\frac{\partial \xi}{\partial r}, \tag{18}$$

then the incompressibility condition (17) is automatically satisfied. After using (18) to replace $u^{(0)}$ and $w^{(0)}$ in the axisymmetric equations, the pressure terms can be eliminated. This results in three equations in the three unknown functions $v^{(0)}$, ξ and $T^{(0)}$. The equations are found using the Maple symbolic computation package, and are sufficiently complicated that no insight is gained by explicitly writing them here.

The boundary conditions for $v^{(0)}$ and $T^{(0)}$ are as before (15), while the no-slip conditions on $u^{(0)}$ and $w^{(0)}$ become

$$\frac{\partial \xi}{\partial r} = \frac{\partial \xi}{\partial z} = 0 \quad \text{on} \quad r = \frac{r_a}{R},\ \frac{r_b}{R} \quad \text{and} \quad z = 0, 1.$$

This condition implies that ξ is constant on the boundaries, and because there is a freedom to choose ξ up to an additive constant, the additional boundary condition is chosen to be

$$\xi = 0 \quad \text{on} \quad r = \frac{r_a}{R},\ \frac{r_b}{R} \quad \text{and} \quad z = 0, 1.$$

5.2 The perturbation equations

The equations that we linearize, to compute the eigenvalues, are called the perturbation equations. We write

$$\mathbf{u} = \mathbf{u}^{(0)} + \hat{\mathbf{u}}, \quad p = p^{(0)} + \hat{p}, \quad T = T^{(0)} + \hat{T}, \tag{19}$$

so that $(\hat{\mathbf{u}}, \hat{p}, \hat{T})$ is a perturbation from the steady axisymmetric solution $(\mathbf{u}^{(0)}, p^{(0)}, T^{(0)})$, where $\mathbf{u}^{(0)} = u^{(0)}\mathbf{e}_r + v^{(0)}\mathbf{e}_\varphi + w^{(0)}\mathbf{e}_z$. By substituting (19) into (10) – (12), and dropping the hats, we obtain the perturbation equations

$$\begin{aligned}
\frac{\partial \mathbf{u}}{\partial t} &= \nu_s \nabla_s^2 \mathbf{u} - \frac{1}{R\rho_0}\nabla_s p - 2\Omega \mathbf{e}_z \times \mathbf{u} + \left(g\mathbf{e}_z - \Omega^2 R r \mathbf{e}_r\right)\alpha T \\
&\qquad - \frac{1}{R}\left(\mathbf{u}^{(0)} \cdot \nabla_s\right)\mathbf{u} - \frac{1}{R}\left(\mathbf{u} \cdot \nabla_s\right)\mathbf{u}^{(0)} - \frac{1}{R}\left(\mathbf{u} \cdot \nabla_s\right)\mathbf{u}, \qquad (20) \\
\frac{\partial T}{\partial t} &= \kappa_s \nabla_s^2 T - \frac{\Delta T}{R}u - \frac{1}{R}\left(\mathbf{u}^{(0)} \cdot \nabla_s\right)T - \frac{1}{R}\left(\mathbf{u} \cdot \nabla_s\right)T^{(0)} - \frac{1}{R}\left(\mathbf{u} \cdot \nabla_s\right)T, \qquad (21) \\
\nabla_s \cdot \mathbf{u} &= 0, \qquad (22)
\end{aligned}$$

with the boundary conditions (15).

The trivial solution $\mathbf{u} = \mathbf{0}$, $p = 0$, $T = 0$ now satisfies these equations, and corresponds to the steady axisymmetric solution of (10) – (12). The linearization of the perturbation equations is not a normal operator.

5.3 The eigenvalue problem

If the perturbation equations (20) – (22) are linearized, and we assume that the unknown functions may be written as

$$\mathbf{u} = \mathbf{u}(r,\varphi,z,t) = e^{\lambda t}\tilde{\mathbf{u}}_m(r,z)e^{im\varphi}, \quad T(r,\varphi,z,t) = e^{\lambda t}\tilde{T}_m(r,z)e^{im\varphi}, \tag{23}$$

with m an integer, then a linear eigenvalue problem is obtained for each azimuthal (or zonal) wave number m. The form of the azimuthal dependence of the unknown functions can be assumed because of the 2π-periodicity in φ.

The linear stability of the axisymmetric solution is found from the eigenvalue problem (see Section 3). In our case, we have a neutral stability curve for each azimuthal wave number m. To one side of each curve (the 'stable' side), all small perturbations of the given wave number decay to zero in the linearized equations, whereas to the other side (the 'unstable' side), there is a perturbation that grows exponentially. In the region of parameter space which is on the stable side of *all* the neutral stability curves, the solution is linearly stable. In the region on the unstable side of *any* of the curves, the solution is unstable. If the parameters are varied such that there is a crossing from the stable region to the unstable region, we can expect a transition from axisymmetric to non-axisymmetric flow.

The eigenvalue problem for the eigenvalues λ and eigenfunctions $\left(\tilde{\mathbf{u}}_m, \tilde{T}_m\right)$, where $\tilde{\mathbf{u}}_m = \tilde{u}_m\mathbf{e}_r + \tilde{v}_m\mathbf{e}_\varphi + \tilde{w}_m\mathbf{e}_z$, is:

$$\begin{aligned}
\lambda\tilde{u}_m &= \nu_s\left(\nabla_m^2\tilde{u}_m - \frac{\tilde{u}_m}{r^2} - \frac{2im}{r^2}\tilde{v}_m\right) + 2\Omega\tilde{v}_m - \frac{1}{\rho_0 R}\frac{\partial\tilde{p}_m}{\partial r} \\
&\qquad -\Omega^2 R\alpha r\tilde{T}_m - \frac{1}{R}\left[\left(\mathbf{u}^{(0)}\cdot\nabla_m\right)\tilde{u}_m + \left(\tilde{\mathbf{u}}_m\cdot\nabla_s\right)u^{(0)} - 2\frac{v^{(0)}\tilde{v}_m}{r}\right] \qquad (24) \\
\lambda\tilde{v}_m &= \nu_s\left(\nabla_m^2\tilde{v}_m - \frac{\tilde{v}_m}{r^2} + \frac{2im}{r^2}\tilde{u}_m\right) - 2\Omega\tilde{u}_m - \frac{im}{\rho_0 Rr}\tilde{p}_m \\
&\qquad -\frac{1}{R}\left[\left(\mathbf{u}^{(0)}\cdot\nabla_m\right)\tilde{v}_m + \left(\tilde{\mathbf{u}}_m\cdot\nabla_s\right)v^{(0)} + \frac{v^{(0)}\tilde{u}_m}{r} + \frac{u^{(0)}\tilde{v}_m}{r}\right] \qquad (25) \\
\lambda\tilde{w}_m &= \nu_s\nabla_m^2\tilde{w}_m + g\alpha\tilde{T}_m - \frac{1}{\rho_0 D}\frac{\partial\tilde{p}_m}{\partial z} - \frac{1}{R}\left[\left(\mathbf{u}^{(0)}\cdot\nabla_m\right)\tilde{w}_m + \left(\tilde{\mathbf{u}}_m\cdot\nabla_s\right)w^{(0)}\right] \qquad (26) \\
\lambda\tilde{T}_m &= \kappa_s\nabla_s^2\tilde{T}_m - \frac{\Delta T}{R}\tilde{u}_m - \frac{1}{R}\left[\left(\mathbf{u}^{(0)}\cdot\nabla_m\right)\tilde{T}_m + \left(\tilde{\mathbf{u}}_m\cdot\nabla_s\right)T^{(0)}\right] \qquad (27) \\
&\frac{\partial\tilde{u}_m}{\partial r} + \frac{\tilde{u}_m}{r} + \frac{im}{r}\tilde{v}_m + \frac{1}{\delta}\frac{\partial\tilde{w}_m}{\partial z} = 0 \qquad (28)
\end{aligned}$$

where

$$\nabla_m^2 = -\frac{m^2}{r^2} + \frac{\partial^2}{\partial r^2} + \frac{1}{r}\frac{\partial}{\partial r} + \frac{1}{\delta^2}\frac{\partial^2}{\partial z^2},$$

and

$$\nabla_m = \mathbf{e}_r\frac{\partial}{\partial r} + \mathbf{e}_\varphi\frac{im}{r} + \mathbf{e}_z\frac{1}{\delta}\frac{\partial}{\partial z}.$$

If $m \neq 0$, it is possible to eliminate $\tilde{p}_m$ and $\tilde{v}_m$. From the incompressibility equation (28), we obtain

$$\tilde{v}_m = \frac{ir}{m}\left(\frac{\partial \tilde{u}_m}{\partial r} + \frac{\tilde{u}_m}{r} + \frac{1}{\delta}\frac{\partial \tilde{w}_m}{\partial z}\right) \tag{29}$$

and from equation (25) we have

$$\begin{aligned}\tilde{p}_m &= -i\frac{\rho_0 R r}{m}\left\{-\lambda\tilde{v}_m + \nu_s\left(\nabla_m^2\tilde{v}_m - \frac{\tilde{v}_m}{r^2} + \frac{2im}{r^2}\tilde{u}_m\right) - 2\Omega\tilde{u}_m \right. \\ &\left. -\frac{1}{R}\left[\left(\mathbf{u}^{(0)}\cdot\nabla_m\right)\tilde{v}_m + \left(\tilde{\mathbf{u}}_m\cdot\nabla_s\right)v^{(0)} + \frac{v^{(0)}\tilde{u}_m}{r} + \frac{u^{(0)}\tilde{v}_m}{r}\right]\right\}. \end{aligned} \tag{30}$$

The resulting three equations in the three remaining unknowns $\tilde{u}_m$, $\tilde{w}_m$, $\tilde{T}_m$ may be written in the form of a generalized eigenvalue problem

$$\lambda\bar{\mathbf{A}}_m\bar{U}_m = \bar{\mathbf{L}}_m\bar{U}_m \tag{31}$$

where

$$\bar{U}_m = \begin{pmatrix} \tilde{u}_m \\ \tilde{w}_m \\ \tilde{T}_m \end{pmatrix}$$

and $\bar{\mathbf{A}}_m$ and $\bar{\mathbf{L}}_m$ are 3×3 matrices of linear operators. If $m = 0$, a stream function method can be used in exactly the same manner as in the calculation of the axisymmetric solution. Again the equations are computed symbolically using Maple.

6 Numerical methods

6.1 Discretization

Since analytic solutions are not possible for either the axisymmetric solution or the eigenvalue problem, the solutions are approximated numerically. Second order centered finite differencing is used to discretize the spatial derivatives. We approximate the value of the unknown functions at the locations of the $N \times N$ grid points in the interior of the domain defined by: $r = r_k$, $1 \leq k \leq N$ and $z = z_l$, $1 \leq l \leq N$, where N, k, l are positive integers, and $r_0 = r_a/R$, $r_{N+1} = r_b/R$, $z_0 = 0$ and $z_{N+1} = 1$. The values of T on the upper and lower boundaries must also be considered as unknowns. This leads to discretized solution vectors of size $3N^2 + 2N$.

Upon discretization, the axisymmetric solution is approximated from a system of nonlinear algebraic equations and the partial differential eigenvalue problems become matrix eigenvalue problems.

6.2 The grid: non-uniform spacing

With the combination of the no-slip boundary conditions and the small parameter (ν) multiplying the second derivative term, boundary layers in the solution of the axisymmetric problem can be expected. For this reason, a scaling method is used to choose the locations of the grid points. This method consists of making a change of coordinates and calculating the solutions on a uniform grid in the new coordinates. The transformation is chosen such that its inverse takes a uniform grid to a grid with many points near the boundary.

The transformation which takes (r, z) to the new coordinates (x, y), is

$$\begin{aligned} r &= \frac{\tan^{-1}(\eta x)}{2\tan^{-1}(\eta/2)} + \frac{1}{2} + \frac{r_a}{R} \\ z &= \frac{\tan^{-1}(\eta y)}{2\tan^{-1}(\eta/2)} + \frac{1}{2} \end{aligned} \tag{32}$$

where η is a scaling factor which determines the magnitude of compression near the boundary. See Figure 3. The domain $r \in [r_a/R, r_b/R]$, $z \in [0, 1]$ goes to $x \in [-1/2, 1/2]$, $y \in [-1/2, 1/2]$. The equations are transformed simply by writing $u(r, z) = u'(x, y)$ (likewise for other functions) and using the chain rule to write the equations in terms of derivatives with respect to x and y.

It turns out that the boundary layers in the eigenfunctions are not as severe as those in the axisymmetric solutions. In fact, significant errors can be introduced into the eigenvalues and eigenfunctions if the grid points in the interior are too sparse. This occurs even if the axisymmetric solutions appear to be well represented. This problem suggests that different scaling factors should be used for the axisymmetric and eigenvalue problems. However, the errors introduced in the interpolation seemed to negate the benefit of using multiple scaling factors. In the calculations presented, we choose the scaling factor $\eta = 6$, which gives qualitatively good results when $N = 20$. It seems that for smaller values of η (for this N), the boundary layer is not well resolved for some values of the parameters Ω and ΔT, while for larger values of η, there are not enough interior points to sufficiently describe the eigenfunctions for all Ω and ΔT.

6.3 Solution techniques

For the computation of the axisymmetric solution we use Newton's method. This method can be combined with a predictor-corrector continuation technique to find the axisymmetric solution for a wide range of parameter values. If $\Omega = 0$ and $\Delta T = 0$, then the trivial solution satisfies the axisymmetric equations. Thus for Ω and ΔT small, the trivial solution is a reasonable prediction of the solution, and Newton's method is used for the correction. For small increments in the parameter values, the previous solution is a reasonable prediction.

To make larger increments in the parameter values, a secant line approximation can be used for the prediction.

Each point on a neutral stability curve is found using an iterative secant method, where the real part of the eigenvalue with largest real part is considered as a function of the parameters. Iteration continues until the magnitude of the real part of the relevant eigenvalue is less than a specified tolerance (10^{-8} for the results presented below).

After discretization, the eigenvalue problem (31) is solved using Arnoldi iteration (Trefethen and Bau, 1997), which computes a specified number of eigenvalues (and corresponding eigenvectors). In particular, we calculate the eigenvalues with smallest magnitude. Although we are interested in the eigenvalue with largest real part when the real part is zero (the critical eigenvalue), experimental results have shown the phase speed of the observed waves to be very slow (see below). The phase speed is given approximately by the imaginary part of the critical eigenvalue, which implies that the magnitude of the critical eigenvalue is small, and, therefore, the eigenvalues with smallest magnitude should correspond with the eigenvalues with largest real part. This hypothesis was tested with $N = 20$ by computing all the eigenvalues. In all such cases, the eigenvalue with smallest magnitude is indeed the eigenvalue with largest real part. This does not guarantee that for smaller grid spacings this is still true, however, the correspondence between the different grid spacings suggests that the assumption is valid. Also, to reduce the risk of error, not only the smallest magnitude eigenvalue is computed, but the p smallest, where in most cases $p = 12$. Note that although this is adequate here, it may not be for other applications.

For the general matrix eigenvalue problem ($\lambda Bv = Av$, where A and B are matrices, v is the eigenvector, λ is the eigenvalue), Arnoldi iteration requires B to be symmetric and positive definite. Unfortunately, this is not the case with the present problem, so it is necessary to invert B to obtain the usual matrix eigenvalue problem (*i.e.* $\lambda v = B^{-1}Av$). This destroys most of the sparseness of the matrices. Taking into account the sparseness, however, still saves a factor of two in computer memory. The non-symmetric property of B is not due to the computation on the non-uniform grid, since there are variable coefficients in the pre-transformed equations.

The discretized (transformed) equations and the entries of the coefficient matrices are computed symbolically using Maple. The results are then transferred to the Matlab numerical computation package, to find the numerical approximations.

6.4 Convergence

For numerical procedures, an important consideration is whether or not the method of approximation is convergent, and if so, to what order is the convergence. A method is called

convergent if the error of the numerical approximation goes to zero as the step size (grid spacing) goes to zero. For the axisymmetric solution, if certain standard assumptions are made about the smoothness of the solutions, and if second order centered differencing is implemented, then there is convergence of order 2 (*i.e.*, the error of the approximation is approximately equal to a constant times h^2, as $h \to 0$, where h is the step size). Convergence also holds for the eigenvalue problem, however, for the present application, the order of the convergence is not known.

Although convergence is an important property of a numerical method, its definition involves a limit as the step size $h \to 0$. Therefore, it is possible that if the step size is not taken small enough, convergence will not be observed. This is particularly evident for the matrix approximation of the eigenvalue problem. It is obvious that the matrix approximation will not be able to contain all the solutions of the continuous problem. (There are at most n eigenvalues of an $n \times n$ matrix where there are an infinite number of eigenvalues of the continuous problem). It could be that when the step size is relatively large, the eigenfunctions corresponding to the critical eigenvalues are not resolved. However, typically, it is the highly oscillatory, high wave number eigenfunctions that the matrix problem is unable to resolve. Since the eigenfunctions corresponding to the critical eigenvalues have relatively low wave numbers and are not highly oscillatory, we expect that these functions are resolved (even if the step size is relatively large), and that the errors in the differencing are relatively small.

Due to the uncertainty introduced when considering finite step size, it is important to look for evidence of convergence in the numerical results themselves. For the approximation of the critical parameter values (the parameter values at the transition) using linear stability analysis, a relatively simple way of investigating convergence consists of inspecting the numerical differences between the approximations at adjacent levels of discretization (grid spacing). If the differences consistently decrease as the grid is refined, then the approximations can be assumed to be convergent. See Section 7 for an example. The results presented below give evidence that the approximation of the transition curve is indeed convergent. A more detailed comparison may also give an estimate of the order of the convergence. However, in our case, the step size could not be taken small enough to obtain such an estimate.

7 Results

The results of our analysis are presented in this section. We will compare our results to the experimental observations of Fein (1973), and, therefore, use the corresponding values of the parameters for the annulus geometry and fluid properties. These are listed in Table 1.

An example of the axisymmetric solution is plotted in Figure 4. Qualitatively, the form of the solution is the same for all values of the parameters. The figure shows that the fluid

velocity in the interior of the fluid is predominantly in the azimuthal direction. The radial velocity is almost zero everywhere except at the upper and lower boundaries, where it is negative and positive, respectively. The vertical velocity is largest at the inner and outer walls, where there is rising at the warmer outer wall and sinking at the cooler inner wall. The azimuthal velocity exhibits an almost linear shear in the vertical in the interior with a positive velocity in the upper half of the annulus and negative velocity in the lower half. The resulting circulation is a convection cell which, due to the Coriolis force, is tilted from the radial plane such that, at the upper and lower boundaries, the inward and outward motion is deflected to the right.

The neutral stability curves are presented in Figure 5. There is a separate curve for each azimuthal wave number. The curves are the points in the parameter space where, for the given wave number, there is one pair of complex conjugate eigenvalues with zero real part while all other eigenvalues associated with that wave number have negative real part. Figure 5 shows the neutral stability curves for the wave numbers $m = 3$ to $m = 8$. Curves for wave numbers from $m = 2$ to $m = 10$ were calculated and it was found that the only critical wave numbers were $m = 3$ to $m = 8$, where the critical wave number is the wave number of the neutrally stable wave at the axisymmetric to non-axisymmetric transition. That is, the neutral stability curves of the wave numbers that are not plotted are always to the right of at least one other curve. It is not possible to calculate the neutral stability curves of all wave numbers, however it can be argued that the higher wave numbers will not be critical in the parameter range of interest. We refer the reader to Lewis (2000) and here justify investigation of only a finite number of wave numbers by comparison with the experimental results. The computations were performed using a 550MHz desktop computer with 256M RAM, running under the Linux operating system. A 25×25 grid was used for the calculations of all curves shown. With the available resources, it was not possible to find detailed neutral stability curves on a finer grid. Approximately 30 points were calculated along each of the curves.

In Figure 6, the curve which delineates the axisymmetric from the non-axisymmetric regimes is plotted. Along this curve it can be seen that there are transitions of the critical wave number. These transitions occur at intersections of the neutral stability curves. Also plotted in Figure 6 is the experimentally observed transition curve taken from Fein (1973), with critical wave number transitions. This is the curve where a transition from the axisymmetric to steady wave flow was observed. All curves are plotted on a log-log graph of Taylor number $\mathcal{T}$ versus thermal Rossby number $\mathcal{R}$. Approximate experimental error bars are also included at selected points along the transition curve. The error bars "reflect the uncertainty due to finite variations of the critical parameter across the transition point as

well as uncertainties associated with measuring one's position in parameter space" (Fein, 1973). The error bars along the upper transition are too small to distinguish and so they are not included. This is due to the log variation of the axes and is not a reflection of more precise measurements.

In Figure 7, is the upper and knee region of the transition. Here, the detail of the intersection of the neutral stability curves is shown. A similar plot of the lower transition would offer no more detail because the curves are very close together.

A number of observations can be made.

- There is a good correspondence between the numerical and experimental results.
- Along the lower transition, the discrepancies between the theoretical and experimental transition curves lie mostly within the experimental error. Along the upper transition, although the discrepancies appear to be small, they still fall beyond the approximated experimental error. This may be due to factors that were not considered in the experimental errors, for instance, the disturbance effects due to the probes that were used to measure the temperature of the fluid. However, the discrepancies may be due to errors in the numerical approximation, or due to errors in the model approximations (*e.g.* the Boussinesq approximation). It is unlikely that the discrepancies are due to the non-normality of the linear part, because if they were, the theoretical curve would be to larger parameter values than the experimental curve.
- There is cusping along the upper transition curve, associated with changes in the critical wave number, in both the experimental and numerical results.
- There is a local maximum of critical wave number ($m = 8$) along both of the lower transition curves.
- It seems that the discrepancies in the wave number transitions along the stability curve are relatively large. This could be due to the difficulty in locating these transitions, both numerically and experimentally.
- The theoretical lower transition curve is not linear on the graph. Fein (1973) believed that his experimental data showed evidence (albeit inconclusive) of this claim.

In fact, all the main features of the transition curves observed in the experiments are replicated with the numerical results. Neither the cusping along the upper transition nor the critical wave number maximum of $m = 8$ along the lower transition has been predicted before in such a realistic model. Miller and Butler (1991), using numerical experimentation (see Section 3), did not locate enough points along the transition curve to reproduce the

curve, and so could not make these predictions. In fact, their results showed a critical wave number maximum of $m = 7$.

A nonlinear bifurcation analysis (Lewis and Nagata, 2001) shows that a non-axisymmetric steady rotating wave bifurcates from the steady axisymmetric solution at the axisymmetric to non-axisymmetric transition. To first order, the wave has the same form as the eigenfunction associated with the critical eigenvalue. Furthermore, the 'drift rate' of the rotating wave at transition can be approximated from the imaginary part of the critical eigenvalue, where the drift rate is the frequency that full wavelengths drift past a fixed point on the annulus. The drift rate ω_d is given by

$$\omega_d = \frac{\omega_c}{m_c}, \tag{33}$$

where ω_c is the imaginary part of the critical eigenvalue and m_c is the wave number of the eigenfunction associated with the critical eigenvalue. The theoretical drift rates at the transition are calculated from (33), and are plotted in Figure 8. The solid line in the figure is a line that is consistent with experimental data (Fein, 1973). Again there is good correspondence. The experimental results do not cover the whole transition curve since some of the wave speeds were judged to be too slow to measure accurately (Fein, 1973).

As mentioned above, an $N \times N$ grid, with $N = 25$, is used for the calculations of all the neutral stability curves that are presented. Neutral stability curves are also calculated for $N = 20$, with good correspondence with the presented results for the lower transition and knee. To test the approximations, calculations with $N = 30$ are also made at several locations along the transition. In all cases, the approximations on the finer grid confirm the validity of the presented results. A comparison of the approximations of the critical parameter values at the different levels of discretization also gives evidence of the convergence of the method of approximation. See Table 2 for an example of one such comparison. The difference between the value for $N = 30$ with the value $N = 25$, is smaller (by almost half) than the difference between the value for $N = 25$ with the value for $N = 20$. Other comparisons reveal similar behaviour. Although this is evidence of convergence, to obtain an estimate of the order of convergence, the calculations would have to be performed with an even finer grid. This is not possible with our available resources. Note, however, that the differences in the approximations of the critical parameter values are quite small. Finally, since the results accurately reproduce the experimental results (see below), we conclude that the approximations are satisfactory. See Lewis (2000) and Lewis and Nagata (2001) for further examples and further discussion of the numerical convergence.

8 Conclusion

In this paper, we use linear stability analysis to determine the transition from axisymmetric steady solutions to non-axisymmetric solutions in a mathematical model of the differentially heated rotating annulus. The relevant eigenvalues cannot be found analytically and therefore numerical approximations are necessary. For two reasons, it is not known *a priori* if the linear stability analysis will make accurate predictions of the transition: (1) errors in the numerical approximation of the eigenvalues may lead to faulty predictions, and (2) it has been suggested that a non-normal linearization of the dynamical equations about the steady solution may also lead to faulty predictions.

For this reason, we study an accurate mathematical model of the annulus, that uses the Navier-Stokes equations in the Boussinesq approximation. We may then validate the predictions *via* quantitative comparison with experimental results. Indeed, we show that the theoretical and experimental results are in good correspondence. The ability of the analysis to replicate the experimental observations not only indicates the validity of the mathematical model and the numerical approximations, but also indicates that the non-normality of the linearization does not preclude the use of linear stability analysis, at least in the present application.

Many features of the experimental transition are duplicated using the predictions of the linear stability analysis. The theoretical transition curve itself is approximately within experimental error for the lower and knee part of the transition. The small discrepancy at the upper transition may be caused by errors in the mathematical model or by factors that were not included in the experimental errors. The critical wave number maximum of $m = 8$ along the lower transition is accurately predicted. For the first time in such an accurate model of the differentially heated rotating annulus, cusping is shown at the upper transition and it is seen that the lower transition is not linear. A previous study (Miller and Butler, 1991), that investigated the annulus configuration of Fein (1973), did not investigate the axisymmetric to non-axisymmetric transition in detail and therefore did not attempt to replicate the experimental results in detail. Furthermore, the study employed numerical experimentation which could not verify the accuracy of linear stability analysis.

In addition to providing a means to quantitatively predict transition curves, linear stability analysis is a starting point for nonlinear bifurcation analysis. The results presented here have been used in a double Hopf bifurcation analysis at the critical wave number transitions (Lewis and Nagata, 2001). The analysis indicates that there is a region in parameter space, adjacent to the critical wave number transitions, where the nonlinear dynamical equations support two stable steady waves. Hysteresis of these waves is predicted and the boundaries of the region of hysteresis are approximated. Also, a first order approximation of the wave

form is given. In principle, this nonlinear analysis can be extended to explore vacillating flow. For the present model, it would be expected that there is a curve in parameter space where the steady waves are neutrally stable. This curve may be the transition curve from wave to vacillating flow.

Finally, this study gives evidence that linear stability analysis may be accurately applied to other complex models, including large scale models of the atmosphere. The fact that accurate numerical approximations are obtained, even when it is necessary to discretize two spatial variables, supports the application of linear stability analysis to many other models where it may have previously been thought of as computationally prohibitive.

References

Chandrasekhar, S., 1961. Hydrodynamic and Hydromagnetic Stability. Oxford University Press, Oxford, UK.

Chossat, P., Iooss, G., 1994. The Couette-Taylor Problem. Vol. 102 of Applied Mathematical Sciences. Springer-Verlag, New York.

Collins, M., James, I., 1995. Regular baroclinic transient waves in a simplified global circulation model of the Martian atmosphere. Journal of Geophysical Research 100 (E7), 14421–14432.

Farrell, B., Ioannou, F., 1996. Generalized stability theory, Part 1: Autonomous operators. Journal of the Atmospheric Sciences 53 (14), 2025–2040.

Fein, J., 1973. An experimental study of the effects of the upper boundary condition on the thermal convection in a rotating cylindrical annulus of water. Geophysical Fluid Dynamics 5, 213–248.

Ghil, M., Childress, P., 1987. Topics in Geophysical Fluid Dynamics. Vol. 60 of Applied Mathematical Sciences. Springer-Verlag, New York.

Hathaway, D., Fowlis, W., 1986. Flow regimes in a shallow rotating cylindrical annulus with temperature gradients imposed on the horizontal boundaries. Journal of Fluid Mechanics 172, 401–418.

Henry, D., 1981. Geometric Theory of Semilinear Parabolic Equations. Vol. 840 of Lecture Notes in Mathematics. Springer-Verlag, Berlin.

Hide, R., Mason, J., 1975. Sloping convection in a rotating fluid. Advances in Geophysics 24, 47–100.

Hignett, P., White, A., Carter, R., Jackson, W., Small, R., 1985. A comparison of laboratory measurements and numerical simulations of baroclinic wave flows in a rotating cylindrical annulus. Quarterly Journal of the Royal Meteorological Society 111, 131–154.

James, I., Jonas, P., Farnell, L., 1981. A combined laboratory and numerical study of fully developed steady baroclinic waves in a cylindrical annulus. Quarterly Journal of the Royal Meteorological Society 107, 51–78.

Kwak, H., Hyun, J., 1992. Baroclinic waves in a shallow rotating annulus with temperature gradients imposed on the horizontal boundaries. Geophysical and Astrophysical Fluid Dynamics 66, 1–23.

Lewis, G., 2000. Double Hopf bifurcations in two geophysical fluid dynamics models. Ph.D. thesis, University of British Columbia.

Lewis, G., Nagata, W., 2001. Double Hopf bifurcations in the differentially heated rotating annulus, submitted to SIAM Journal on Applied Mathematics.

Lewis, S., 1992. A quasi-geostrophic numerical model of a rotating internally heated fluid. Geophysical and Astrophysical Fluid Dynamics 65, 31–55.

Lu, H., Miller, T., Butler, K., 1994. A numerical study of wavenumber selection in the baroclinic annulus flow system. Geophysical and Astrophysical Fluid Dynamics 75, 1–19.

Maslowe, S., 1985. Shear flow instabilities and transition. In: Swinney, H., Gollub, J. (Eds.), Hydrodynamic Instabilities and the Transition to Turbulence. Vol. 45 of Topics in Applied Physics. Springer-Verlag, New York, pp. 181–228.

Miller, T., Butler, K., 1991. Hysteresis and the transition between axisymmetric flow and wave flow in the baroclinic annulus. Journal of the Atmospheric Sciences 48 (6), 811–823.

Mo, J., Zheng, Y., Antar, B., 1995. A numerical analysis of strongly nonlinear baroclinic instability. Fluid Dynamics Research 16, 251–273.

Mundt, M., Hart, J., Ohlsen, D., 1995. Symmetry, sidewalls, and the transition to chaos in baroclinic systems. Journal of Fluid Mechanics 300, 311–338.

Trefethen, L., 1997. Pseudospectra of linear operators. SIAM Review 39 (3), 383–406.

Trefethen, L., Bau, D., 1997. Numerical Linear Algebra. Society for Industrial and Applied Mathematics, Philadelphia.

Trefethen, L., Trefethen, A., Reddy, S., Driscoll, T., 1993. Hydrodynamic stability without eigenvalues. Science 261, 578–584.

Wiggins, S., 1990. Introduction to Applied Nonlinear Dynamical Systems and Chaos. Vol. 2 of Texts in Applied Mathematics. Springer-Verlag, New York.

r_a	3.48	cm
r_b	6.02	cm
R	2.54	cm
D	5	cm
ν	$1.01e^{-2}$	cm^2/sec
κ	$1.41e^{-3}$	cm^2/sec
α	$2.06e^{-4}$	$1/^\circ$ C
ρ_0	0.998	gm cm^3
T_0	20.0	$^\circ$ C
g	980	gm/cm^3

Table 1: The annulus geometry and fluid properties used in the analysis, after Fein (1973). See text for definitions of symbols.

N	Ω_0	ΔT_0
20	0.800	0.396
25	0.800	0.383
30	0.800	0.375

Table 2: An example of the approximate critical parameter values for different values of N, where the approximations are made on an $N \times N$ grid and Ω_0 and ΔT_0 are the critical parameter values. For this example, Ω was held fixed while ΔT was varied.

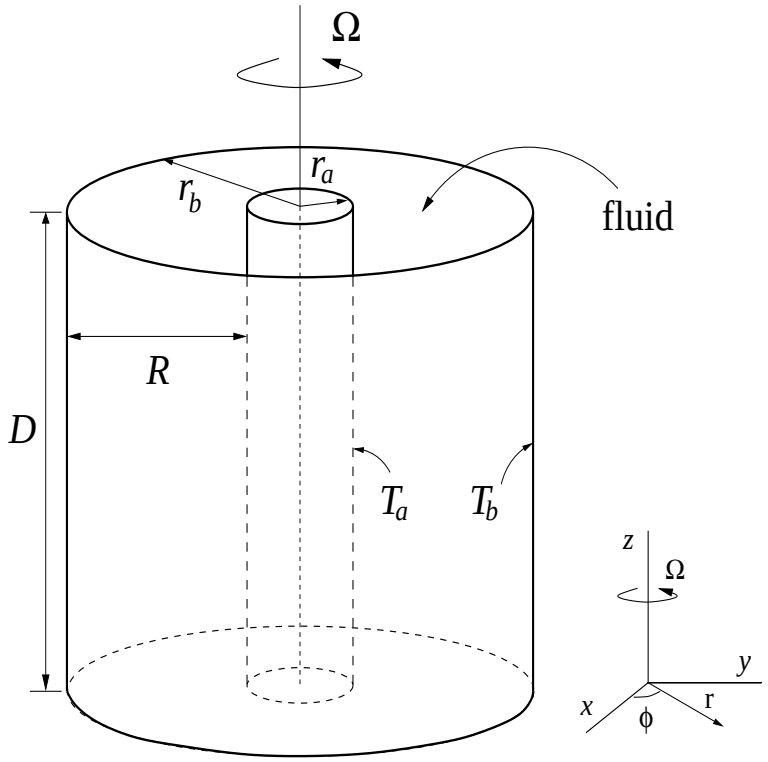

Figure 1: The differentially heated rotating annulus experiment, where the annulus is rotated at rate Ω and the inner wall is held at the fixed temperature T_a and the outer wall at temperature T_b, creating a differential heating. r_a and r_b are the radii of the inner and outer cylinders, $R = r_b - r_a$, and D is the height of the annulus.

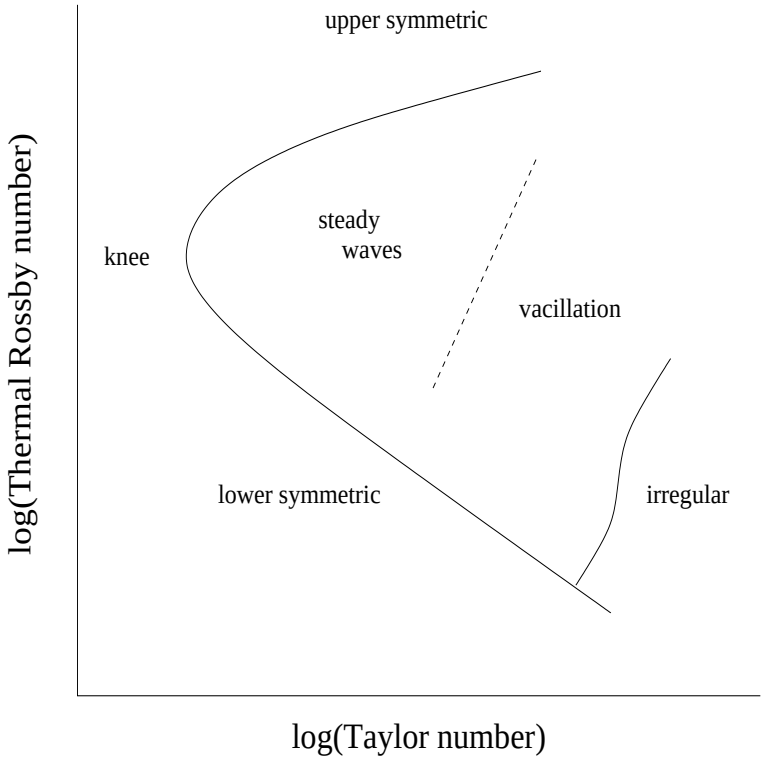

Figure 2: A schematic diagram depicting general experimental results. See *e.g.* Hide and Mason (1975). To the left of all the curves is the axisymmetric regime which is separated into three (dynamically similar) regions: lower symmetric, knee, and upper symmetric. To the right of the curve is the non-axisymmetric regime which is separated into three dynamically distinct regimes: steady waves, vacillation and irregular flow.

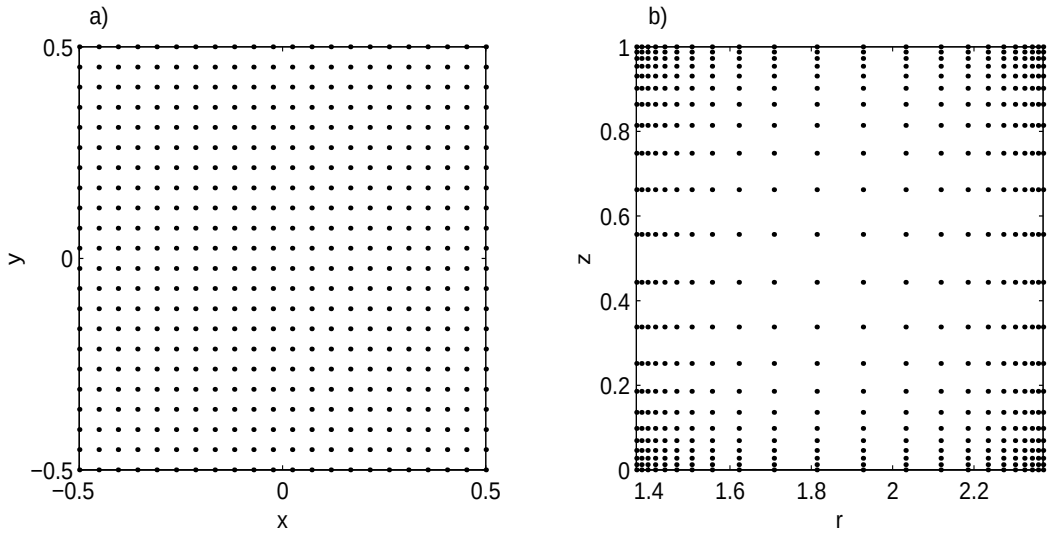

Figure 3: The transformation of the grid points. (a) A uniform grid (equally spaced grid points) of size 20×20 (b) the grid obtained by applying the change of coordinates (32) with $\eta = 6$.

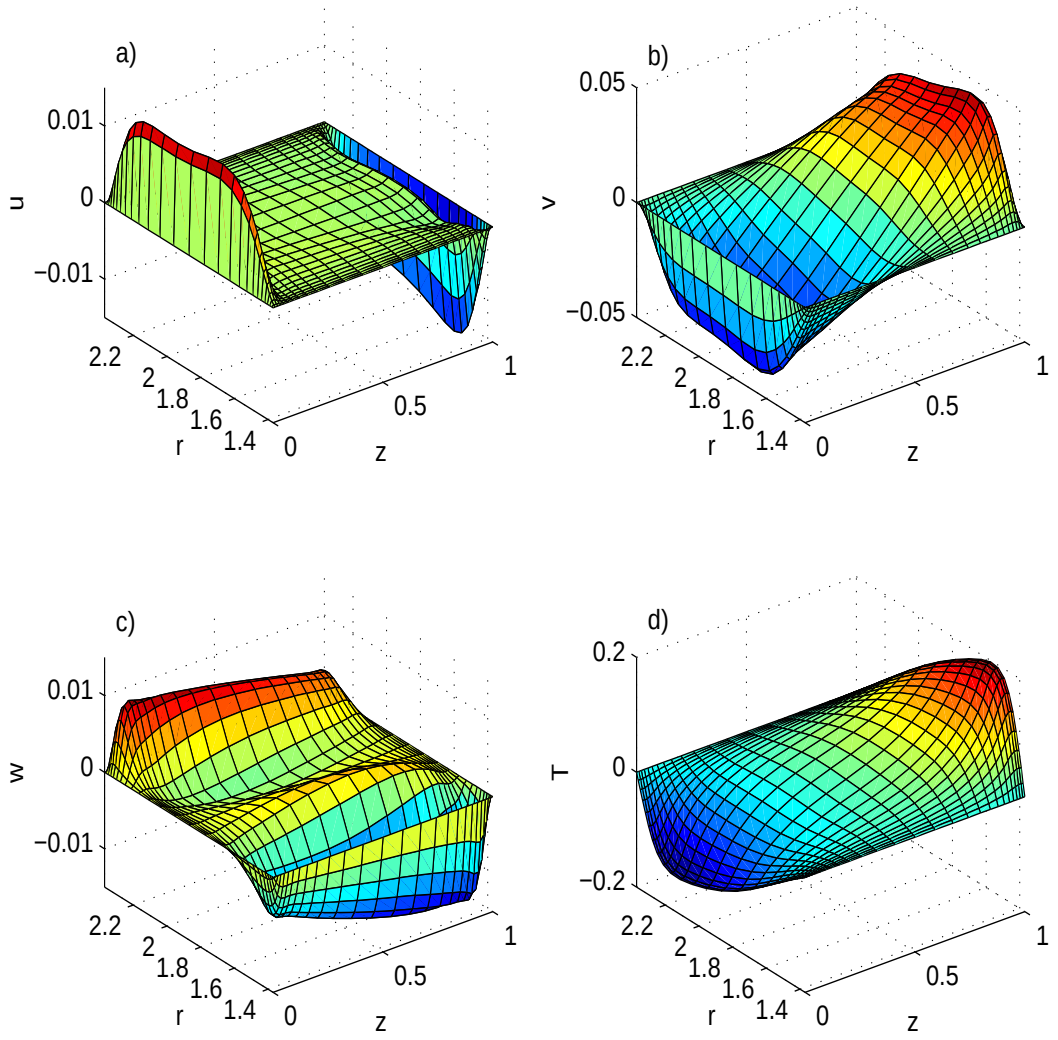

Figure 4: The axisymmetric solution: (a) u the fluid velocity in the radial direction, (b) v the fluid velocity in the azimuthal direction, (c) w the fluid velocity in the vertical direction, and (d) T the deviation of the temperature of the fluid from $\Delta T\,(r - r_a/R) + T_a$. This solution is calculated on a 25×25 grid and is observed at $\Omega = 0.8169$ and $\Delta T = 0.3820$.

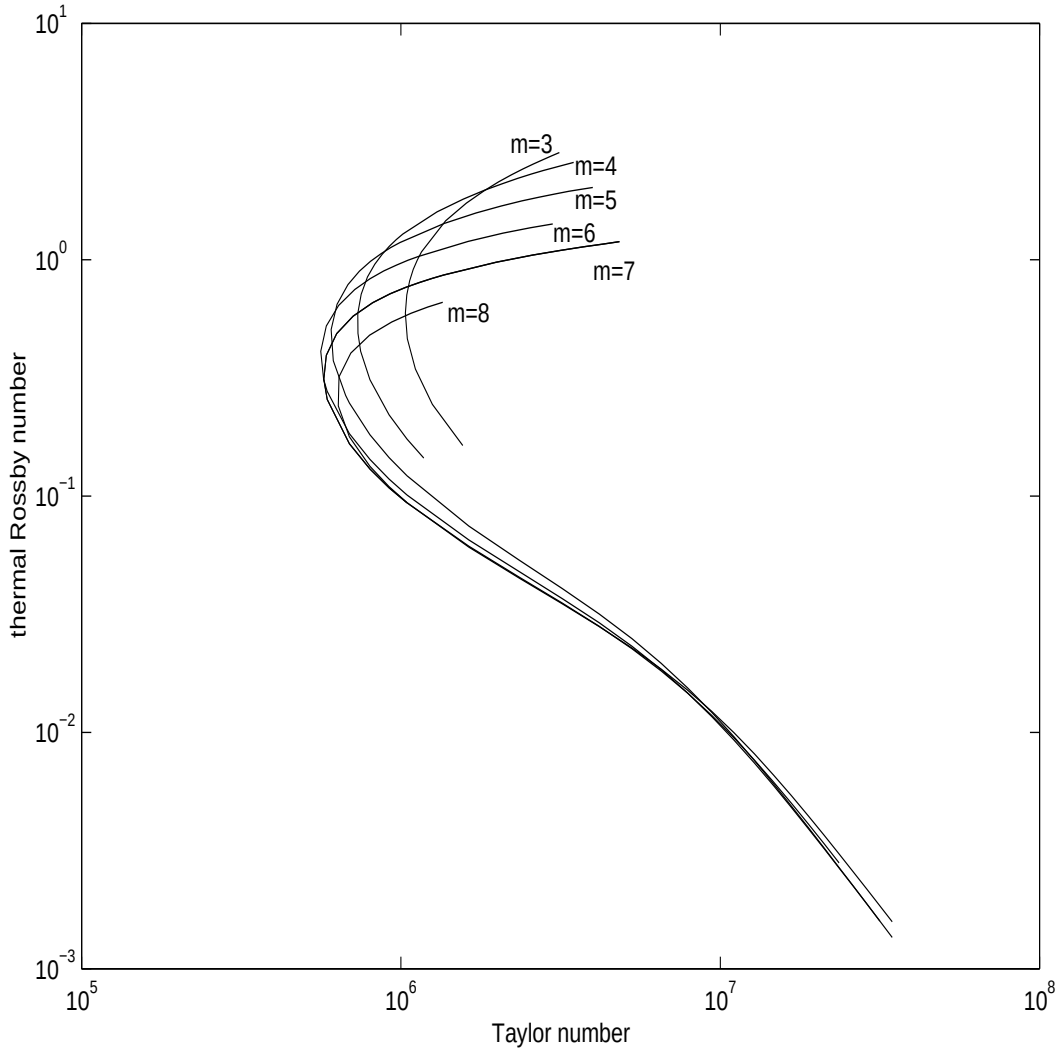

Figure 5: Neutral stability curves are plotted for the wave numbers $m = 3$ to $m = 8$. The curves are calculated by finding the parameter values where, for each m, the eigenvalues of (31) all have negative real part except one with zero real part. The curves are plotted on a log-log graph of thermal Rossby number versus Taylor number.

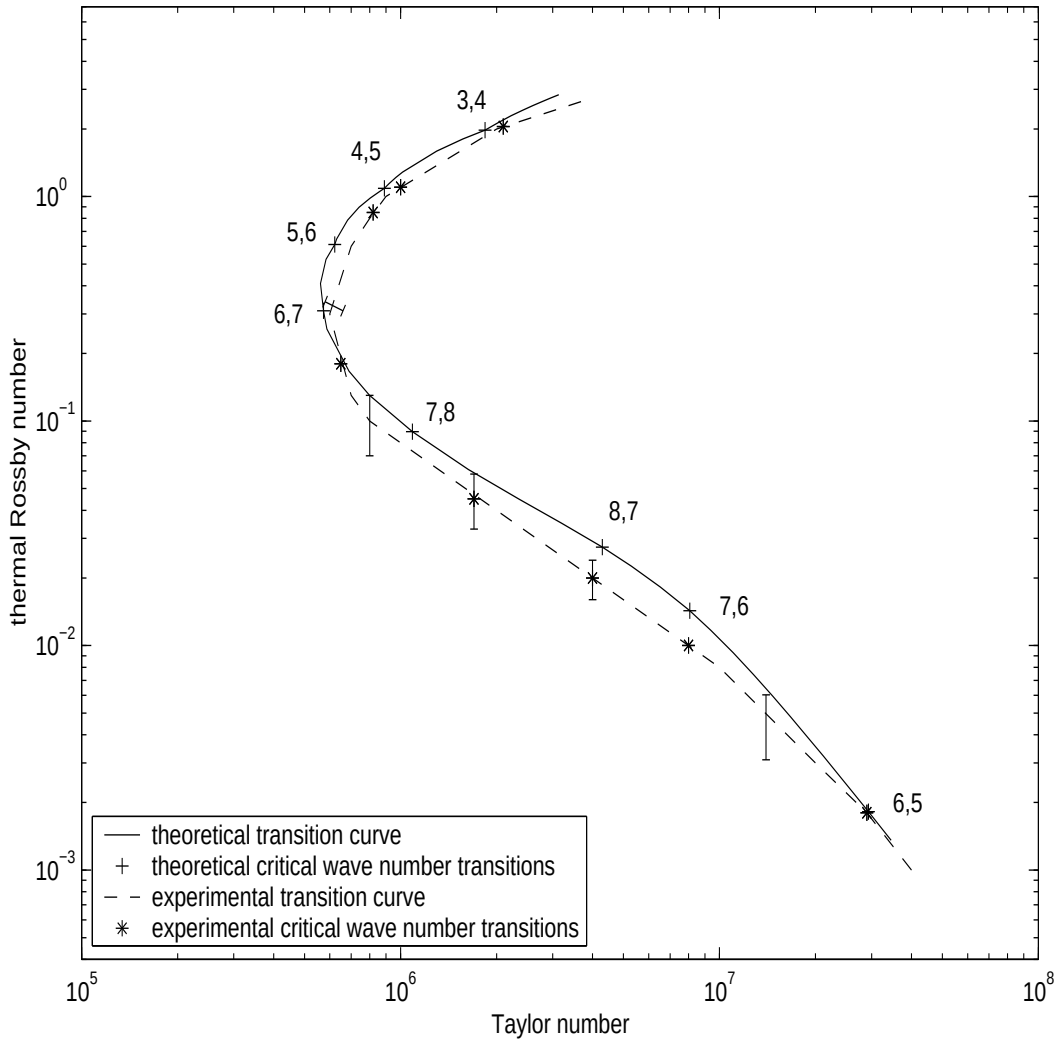

Figure 6: Transition curves for theory and experiment delineating the axisymmetric from the non-axisymmetric regimes. The critical wave number transitions, labelled as m_1, m_2, are also plotted along the curve. Experimental error bars are included at selected points along the experimental transition curve.

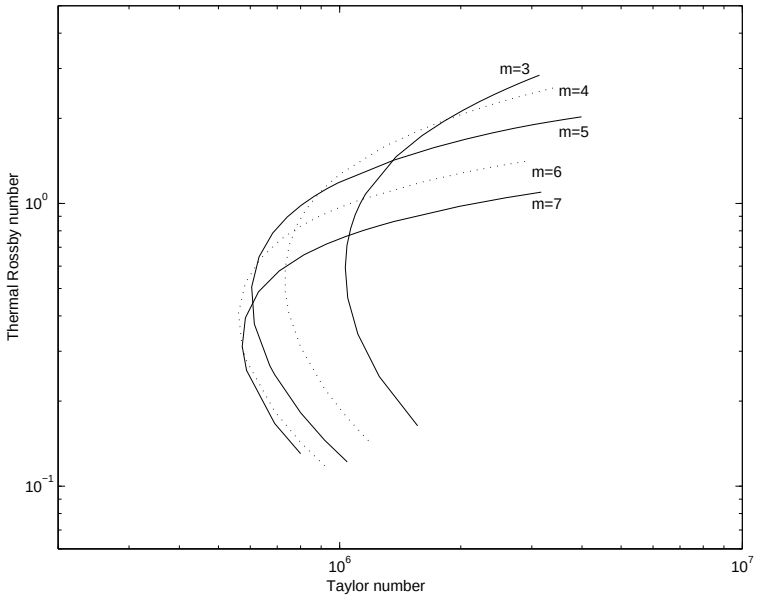

Figure 7: Neutral stability curves: upper transition. Same as Figure 5, but only top part is shown.

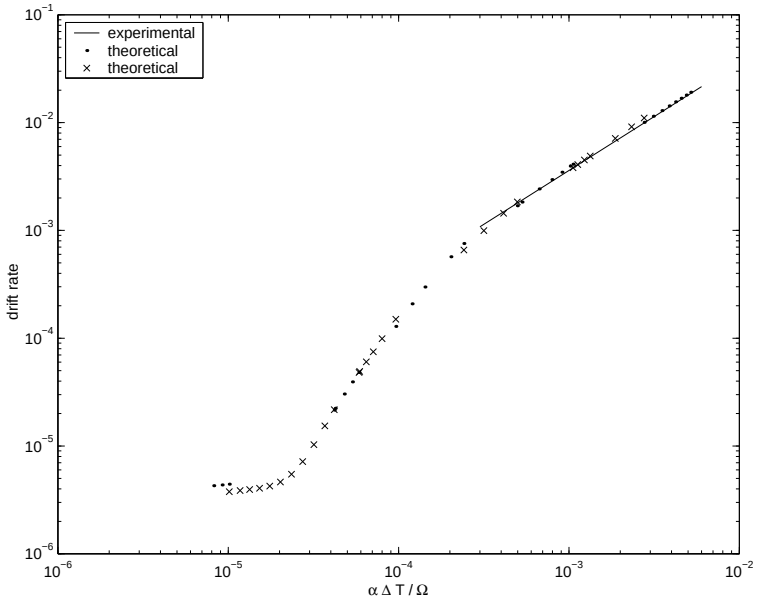

Figure 8: Theoretical and experimental drift rates of steady rotating waves at transition, where the drift rate is the frequency that full wavelengths drift past a fixed point on the annulus. Theoretical drift rates are labelled with both x's and dots so that the results from neighbouring wave numbers can be distinguished (that is, transitions from x's to dots, and visa versa, correspond to wave number transitions along the transition curve). The solid line is consistent with the experimental results (within experimental error) of Fein (1973). Theoretical results are calculated from (33). $\alpha\Delta T/\Omega$ is the intensity of the 'thermal wind', see Fein (1973).